ISBN: 978-3-95450-247-9 ISSN: 2673-5490 doi: 10.18429/JACoW-IPAC2024-MOPR76

STUDIES OF PHOTOEMISSION IN THE HIGH-FIELD REGIME IN AN X-BAND RF GUN *

G. Chen†, D. Doran, S. Kim, W. Liu, A. Ody, P. Piot, J. Power, C. Whiteford, E. Wisniewski
Argonne National Laboratory, Lemont, IL, USA
C. Jing[1], E. Knight, S. Kuzikov, Euclid Techlabs LLC, Bollingbrook, IL, USA
E. Frame, X. Lu[1], G. Ha[1], Northern Illinois University, DeKalb, IL, USA
[1] also at Argonne National Laboratory, Lemont, IL, USA

Abstract

A program is underway at the Argonne Wakefield Accelerator (AWA) facility, in collaboration with Euclid Techlabs and Northern Illinois University (NIU), to develop a GV/m-scale photocathode gun, to produce bright electron bunches. The novel X-band (11.7 GHz) photoemission gun (Xgun) powered by short rf-pulse (9 ns) has already demonstrated peak fields of 400 MV/m in our previous work. As a first step towards achieving a complete understanding of the Xgun's performance in the high-field regime, we performed the Schottky scan across a large range of operating fields on the cathode surface from 60 MV/m to 320 MV/m. In this study, we are trying to get a comprehensive understanding of the Schottky scan data through systematic beam simulations.

INTRODUCTION

The development of high-brightness photoinjectors is a key technology for a variety of scientific applications including future linear colliders, next-generation free-electron lasers (FELs) [1], compact X-ray sources [2], and ultrafast electron diffraction or microscopy (UED/UEM) [3, 4]. To generate a high-brightness beam (i.e., high charge and low emittance), there are two main methods: 1) minimizing the thermal emittance of the cathode, which sets the lowest achievable emittance, and 2) preserving the low-emittance electron bunch after photoemission through high-gradient acceleration. While research in novel cathode materials could contribute to the first method, at AWA (Argonne Wakefield Accelerator facility), we are pursuing the latter approach. Moreover, previous studies have shown that the brightness ($\mathcal{B}$) of the beam increases in proportion to the accelerating gradient (E) applied on the cathode surface, given by the relationship $\mathcal{B} \propto E^m/MTE$ where m depends on the beam's transverse-to-longitudinal aspect ratio and MTE is the mean-transverse energy of the cathode [5].

A ultra-high peak field of ~ 400 MV/m on the cathode surface has already been achieved in a novel X-band photogun (Xgun) [6]. As the first step toward the generation of bright beam, it is important to get a comprehensive understanding in the emission processes in this unprecendented high-field regime. In this work, we conducted a series of rf phase scans – i.e. scanning the laser launch phase with respect to the rf-gun field – for field in the range of [60, 320] MV/m, and compared with the simulations.

EXPERIMENTAL SETUP

In Fig. 1, a schematic diagram of the upstream section of the Xgun beamline is presented, which is used for the rf phase scan measurements. A few key elements of the beamline include the 1.5-cell Xgun (detailed rf properties are discussed in Refs. [6,7]), an repurposed solenoid modified to reduce the residual B_z field on cathode surface, an integrated current transformer (ICT) and beam position monitor (BPM) for charge measurements. Owing to the better sensitivity of BPM pickup antennae, the BPM (once cross-calibrated against the ICT signal at higher charges) can measure low-charge electron bunches.

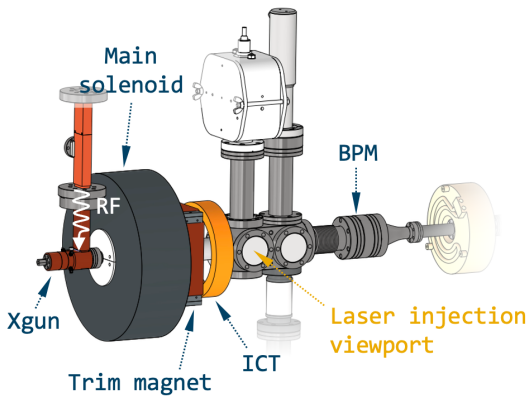

Figure 1: Schematic diagram of the upstream section of the Xgun beamline, which is designated for phase scan measurements.

The Xgun phase scan was conducted by adjusting the laser injection phase which is controlled by a changing the optical path using an optical-delay stage and thus changing the relative arrival time of the laser on the cathode with respect to the rf field. The solenoid strength was tuned at each gradient level for achieving maximum electron capture, and the emitted electron charge was measured using the ICT (and cross-checked by BPM in the downstream). The nominal operation parameters are listed in Table 1.

* This work is supported by the U.S. DOE, under award No. DE-SC0022010 to NIU, DOE SBIR grant No. DE-SC0018709 at Euclid Techlabs LLC, and contract No. DE-AC02-06CH11357 with ANL. At ANL, this work is partially supported by Laboratory Directed Research and Development (LDRD) funding.
† b288079@anl.gov

ISBN: 978-3-95450-247-9 ISSN: 2673-5490 doi: 10.18429/JACoW-IPAC2024-MOPR76

Table 1: List of the Operation Parameters

Parameter	Value
Laser $\sigma_{x,y}$	0.5 mm
Laser pulse duration (FWHM)	300 fs
Laser wavelength	262 nm
Gradient on cathode	60 MV/m to 320 MV/m
Solenoid peak field B_z	0.09 T to 0.22 T

XGUN RF PHASE SCANS: MEASUREMENTS AND SIMULATIONS

The rf phase scan (or Schottky scan) is studied by simulating the electron bunch charge as a function of the rf phase of the Xgun. In ASTRA, the initiated bunch charge (Q) is evaluated as the following equation:

$$Q = Q_0 + S_1\sqrt{E} + S_2 E \tag{1}$$

Here S_1 [nC·$\sqrt{\text{m/MV}}$] and S_2 [nC·m/MV] are the Schottky-strength coefficients, and E is the total electric field on the cathode surface. In practice, the electric field in an rf gun is a composite of multiple field sources (as described in Eq. (2). The primary contribution is the gun rf field ($E_0 \sin(\varphi_{\text{rf}})$), other contributions include the space charge shielding field (E_{sc}) which is opposite to the beam accelerating direction, and electric field introduced by the physical/chemical roughness variation ($E_{\text{roughness}}$) on the cathode surface [8, 9].

$$E = E_0 \sin(\varphi_{\text{rf}}) + E_{\text{sc}} + E_{\text{roughness}} \tag{2}$$

Simulation Setup

In ASTRA, both the rf field and the space charge field are explicitly considered in the nominal algorithm. In this study, the 3D field map of the Xgun (simulated by CST) is incorporated into the beam dynamics simulations. However, simulating the electric field introduced by surface roughness ($E_{\text{roughness}}$) can be computationally intensive in CST, as representing sub-μm scale surface features accurately often requires a much finer mesh resolution comparing to the typical size of X-band structures. Therefore, we conduct a numerical analysis of the $E_{\text{roughness}}$ using a reduced model. Referring the work by Gevorkyan *et al.* [9] and Bradley *et al.* [8], a sinusoidal surface $z = a\cos(px)$ was employed to model physical surface roughness variations, where a represents the surface roughness and p is related to the peak-to-peak separation of the surface features. The extended 3D $\boldsymbol{E}(x, y, z)$ is expressed as follows,

$$\begin{aligned} E_x &= E_0 p(a/2) e^{-pz} \sin(px)\cos(py), \\ E_y &= E_0 p(a/2) e^{-pz} \sin(py)\cos(px), \\ E_z &= E_0 pa e^{-pz} \cos(px)\cos(py). \end{aligned} \tag{3}$$

With the measured roughness, where a is of 0.4 µm and p is estimated to be $2\pi/50$ µm^{-1}, the cathode field map was constructed within a confined volume of 10 mm by 10 mm by 0.1 mm (x, y, z), where the transverse size is comparably large to cover the laser area. This cathode field map was then imported into ASTRA as a separate 3D cavity field. As shown in Fig. 2, the roughness field is located at $z = 0$, and a fixed phase shift is applied between the Xgun field and the roughness field.

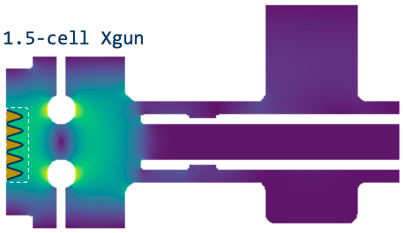

Figure 2: Field distribution of the Xgun. A 3D sinusoidal surface (shown in the dashed box) on the cathode surface is included in the simulation to model the surface roughness.

With both the cathode and cavity field maps imported and the real Xgun geometry configured as an aperture (using the properties of annealed copper to evaluate secondary electron emission), together with all operation parameters (listed in Table 1) set in the simulation, the next step is to determine the Schottky coefficients (S_1, S_2) and the initial bunch charge (Q_0) in Eq. (1). Using the measured low gradient (60 MV/m) phase scan data (Fig. 3(e)) as a reference, the parameters S_1, S_2 and Q_0 were optimized in order to have a good match to the experimental data since ASTRA, since the phase scan at this gradient level is well benchmarked [10]. The optimized fit values were found to be, $S_1 \simeq 0.003$, $S_2 \simeq 0$, and $Q_0 = 5.6$ pC. These values were kept the same and were applied across all higher gradient simulations.

Results and Discussion

The measured data of phase scan at different gradients are shown in Fig. 3 (a-e) (solid purple lines). For comparison, a few sets of simulations were conducted: 1) Simulations with roughness field included as described in Eq. (2), 2) simulations with only the rf field and space charge field, ignoring the roughness field, and 3) phase scans conducted without any apertures (i.e. no physical constraints imposed by the cavity structure, the co-axial coupler and the beam pipe etc.).

At all gradients, simulations that include the roughness field suggest a better agreement with the measured data (in terms of simulated charge levels and the overall phase scan trend), especially these simulations demonstrate a smoother emission turn-on near the zero phase comparing to the sharp turn-on when the roughness field is excluded.

However, a noticeable discrepancy was observed at the high gradient of 320 V/m. Considering possible measurement errors and system jitters, such a significant discrepancy may suggest a different emission mechanism that results in additional electron emission at certain phases. A possible source of emission may be attributed to photo-assisted field emission. Such emission process is widely used in mi-

ISBN: 978-3-95450-247-9 ISSN: 2673-5490 doi: 10.18429/JACoW-IPAC2024-MOPR76

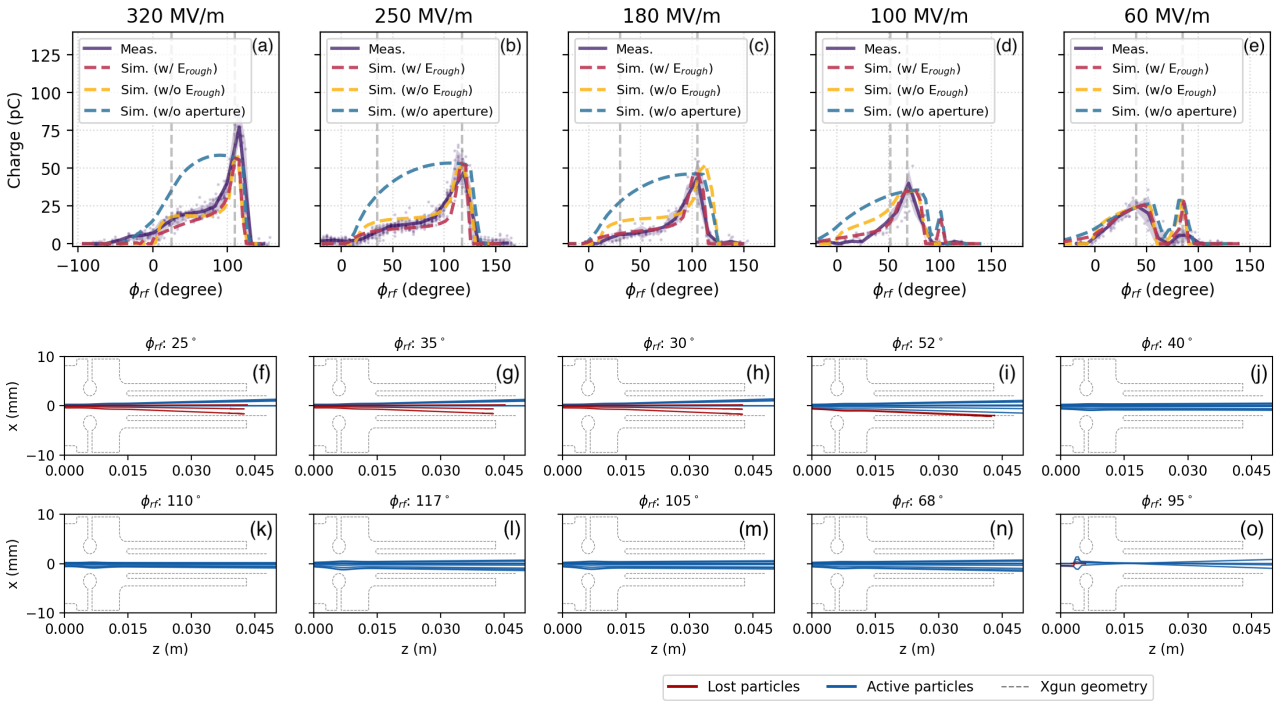

Figure 3: (a)-(e) Phase scan measurement (solid lines) and simulation (dashed lines) comparisons at different gradients of 320 MV/m, 250 MV/m, 180 MV/m, 100 MV/m and 60 MV/m, respectively; the red dashed line is the simulation include all effects E_{rf}, E_{sc} and $E_{\mathrm{roughness}}$, yellow dashed lines consider only E_{rf} and E_{sc}, and blue dashed lines exclude the aperture constraint in ASTRA. The bottom two rows describe the selected particle trajectories (x vs. z) for the two phases marked (vertical dashed grey) in the respective top figure of each column. In (f)-(o), the thin blue lines represent the trajectories of active particles, and the thin red lines represent the lost particles during the beam tracking. The thin dashed lines depict the Xgun geometry, which is employed as the aperture constraint in the simulation.

croscopy area, where ultra-high gradients (GV/m-level) are generated from sharp tips that greatly enhance the electric field; then together with sufficient laser energy to allow the electron tunneling through [11]. The field emission model has been described by the Fowler-Nordheim equation [12],

$$J(E) = a\frac{\beta^2 E^2}{\phi_{\mathrm{eff}}}\exp\left(-b\frac{\phi_{\mathrm{eff}}^{3/2}}{\beta E}\right) \tag{4}$$

where $J(E)$ is the emissison current density, a and b are Fowler-Nordheim constants, β is the field enhancement factor, and ϕ_{eff} is the effective work function. To have a rough estimate on the charge contribution from photo-assisted field emission in our case, β is assumed to be small ($\lesssim 2$) as no pure- emission was observed during the experiment. The work function of copper is estimated to be 4.6 eV, which will be lowered by the Schottky effect at a surface field of 320 MV/m. Additionally, copper has a high absorption rate at UV range, with approximately 65% at the 262 nm UV wavelength [13], which further contributes in reducing the work function. The estimated charge can reach up to several tens of pico-coulombs, peaking at the phase of 90°, with similar longitudinal profile as the photo-emitted electrons. More studies are desired to reveal the detailed emission mechanisms at high-gradient levels.

Additionally, the simulated results shown in Fig. 3 (a-e) revealed a beam clipping issue with the current laser spot size, particularly when compared to the sets without physical constraints. Figure 3 (f-o), which describes particle trajectories in the gun at two different rf phases for each gradient, indicates that the clipping happens near the gun's exit in the coupler region. This issue is expected to be improved in the upcoming version of the Xgun, where the rf coupler is moved to the back of the half-cell.

CONCLUSION

In conclusion, we explored emission mechanisms across a gradient from 60 MV/m to 320 MV/m through detailed phase scans and systematic simulations. Discrepancies at the gradient of 320 MV/m may indicate additional emission mechanisms, possibly photo-assisted field emission. Future improvements in the Xgun design, particularly relocating the rf coupler, are anticipated to enhance performance by addressing beam clipping issues at the gun exit. Likewise, the availability of an optical parametric amplified in the future will allow more detailed exploration of photoemission in the high-field regime enabled by the short-RF-pulse Xgun.

ISBN: 978-3-95450-247-9 ISSN: 2673-5490 doi: 10.18429/JACoW-IPAC2024-MOPR76

REFERENCES

[1] P. Emma *et al.* ,"First lasing and operation of an ångstrom-wavelength free-electron laser", *Nat. Photonics* vol. 4, p. 641, 2010.

[2] W. S. Graves *et al.*, "Compact x-ray source based on burst-mode inverse Compton scattering at 100 kHz", *Phys. Rev. Spec. Top. Accel Beams*, vol. 17, p. 120701, 2014. doi:10.1103/PhysRevSTAB.17.120701

[3] F. Qi *et al.*, "Breaking 50 Femtosecond Resolution Barrier in MeV Ultrafast Electron Diffraction with a Double Bend Achromat Compressor", *Phys. Rev. Lett.*, vol. 124, p. 134803, Mar. 2020. doi:10.1103/physrevlett.124.134803

[4] R. K. Li and P. Musumeci, "Single-Shot MeV Transmission Electron Microscopy with Picosecond Temporal Resolution", *Phys. Rev. Appl.*, vol. 2, p. 024003, Aug. 2014. doi:10.1103/physrevapplied.2.024003

[5] D. Filippetto, P. Musumeci, M. Zolotorev, and G. Stupakov, "Maximum current density and beam brightness achievable by laser-driven electron sources", *Phys. Rev. ST Accel. Beams*, vol. 17, p. 024201, Feb. 2014. doi:10.1103/physrevstab.17.024201

[6] W. H. Tan *et al.*, "Demonstration of sub-GV/m accelerating field in a photoemission electron gun powered by nanosecond X-band radio-frequency pulses", *Phys. Rev. Accel. Beams*, vol. 25, p. 083402, 2022.

[7] S. V. Kuzikov *et al.*, "An X-Band Ultra-High Gradient Photoinjector,"in *Proc. IPAC'21*, Campinas, Brazil, May 2021, pp. 2986–2989. doi:10.18429/JACoW-IPAC2021-WEPAB163

[8] D. J. Bradley *et al.*, "The transverse energy of electrons emitted from GaAs photocathodes", *J. Phys. D: Appl. Phys.*, vol. 10 p. 111, 1977. doi:10.1088/0022-3727/10/1/013

[9] G. S. Gevorkyan *et al.*, "Effects of physical and chemical surface roughness on the brightness of electron beams from photocathodes", *Phys. Rev. Accel. Beams*, vol. 21, p. 093401, 2018. doi:10.1103/PhysRevAccelBeams.21.093401

[10] J. H. Han *et al.*, "Secondary electron emission in a photocathode rf gun", *Phys. Rev. ST Accel. Beams*, vol. 8, p. 033501, 2005. doi:10.1103/PhysRevSTAB.8.033501

[11] M. Lee, "Field Emission of Hot Electrons from Tungsten", *Phys. Rev. Lett.*, Vol. 30, No. 24 pp. 1193-1196, 1973. doi:10.1103/PhysRevLett.30.1193

[12] R. H. Fowler and L. Nordheim, "Electron emission in intense electric fields", *Proceedings of the Royal Society of London. Series A (Proc. R. Soc. A)*, Vol. 119, pp. 173-181, 1928. doi:10.1098/rspa.1928.0091

[13] S. Babar and J. H. Weaver, "Optical constants of Cu, Ag, and Au revisited,"*Appl. Opt.*, vol. 54, pp. 477–481, 2015.